

# PHYSICAL REVIEW B

## CONDENSED MATTER

THIRD SERIES, VOLUME 42, NUMBER 16 PART A

1 DECEMBER 1990

### EPR study of $\text{Fe}^{3+}$ in $\alpha$ -quartz: Further lithium-compensated centers

Deok Choi

*Department of Chemistry, University of Saskatchewan, Saskatoon, Saskatchewan, Canada S7N 0W0  
and Department of Physics, Myong Ji University, Yongin, Kyunggi-do, 449-728, South Korea*

John A. Weil\*

*Department of Chemistry, University of Saskatchewan, Saskatoon, Saskatchewan, Canada S7N 0W0*

(Received 1 August 1990)

$\text{Fe}^{3+}$  ( $S = \frac{5}{2}$ ) centers in synthetic  $\alpha$ -quartz, designated by  $S'_1$  and  $S''_1$  by previous workers, which are very similar to the previously studied center  $[\text{FeO}_4/\text{Li}]^0_\alpha$  (called  $S_1$ ), have been examined at temperatures around 35 K via an  $X$ -band electron-paramagnetic-resonance study. Hyperfine signals due to the  $^7\text{Li}$  nucleus were detected for both centers, establishing their alkali-metal-ion content. The spin-Hamiltonian parameters were determined, allowing for anisotropy of the  $g$  factor as well as  $[g, D, A(^7\text{Li}), P(^7\text{Li})]$ -matrix noncoaxiality, and including high-spin terms of the form  $S^4$ . Evaluation of the results indicates that the lithium  $1+$  ion is present interstitially near to the substitutional  $\text{Fe}^{3+}$  ion (located at a  $\text{Si}^{4+}$  site) on the same crystal twofold axis, for all three centers:  $S_1$ ,  $S'_1$  and  $S''_1$ . The designations  $[\text{FeO}_4/\text{Li}]^0_\alpha$  and  $[\text{FeO}_4/\text{Li}]^0_{\alpha'}$  are proposed for the centers  $S_1$  and  $S'_1$ , respectively. The relative concentrations of these centers appear to depend sensitively on the growth regions within each crystal.

## I. INTRODUCTION

Recently, we have undertaken a series of detailed electron-paramagnetic-resonance (EPR) and some electron-nuclear double-resonance (ENDOR) studies of the various  $\text{Fe}^{3+}$  centers in crystalline  $\alpha$ -quartz.<sup>1-7</sup> The center  $S_1$ , which exists frequently in cultured iron-doped quartz, as well as in natural amethyst and citrine quartz crystals,<sup>3,8-10</sup> was shown to be a lithium-compensated  $\text{Fe}^{3+}$  center, called  $[\text{FeO}_4/\text{Li}]^0_\alpha$ .<sup>3,6</sup> In this center, an  $\text{Fe}^{3+}$  ion substitutes for a  $\text{Si}^{4+}$  ion and a charge-compensating  $\text{Li}^+$  ion is located interstitially, both on the same twofold axis in  $\alpha$ -quartz. Such  $C_2$  local symmetry of this center continues down to 4 K. A second type of a Li-compensated  $\text{Fe}^{3+}$  center, denoted by  $[\text{FeO}_4/\text{Li}]^0_\beta$ , shows  $X$ -band EPR spectra with  $C_1$  symmetry at around 20 K and approaching  $C_2$  symmetry at higher temperatures (above 160 K).<sup>4</sup>

Two other centers, designated by  $S'_1$  and  $S''_1$ , have been found to be similar to  $S_1$  in their spin-Hamiltonian parameters and principal axes. The fine-structure parameters  $D$ ,  $E$ , and  $F$  for these two centers at room temperature were estimated previously, assuming an isotropic  $g$  value,<sup>11</sup> and the temperature dependence of these parameters was investigated from 90 to 300 K.<sup>12</sup> However, the compensating ions of these centers were not then

identified. In the present paper, we report the results of a reexamination on the two centers  $S'_1$  and  $S''_1$ , at approximately 35 K. The spin-Hamiltonian parameters for both centers, particularly including the hyperfine and the quadrupole matrices due to the  $^7\text{Li}$  nucleus, have now been determined. Both centers show  $C_2$  local symmetry from 300 down to 35 K. Herein, the two centers  $S'_1$  and  $S''_1$  are called  $[\text{FeO}_4/\text{Li}]^0_{\alpha'}$  and  $[\text{FeO}_4/\text{Li}]^0_{\alpha''}$ , respectively, and at times the abbreviations  $\alpha$ ,  $\alpha'$ , and  $\alpha''$  will be used.

## II. EXPERIMENTAL

The synthetic colorless and transparent  $\alpha$ -quartz crystal primarily used in this investigation was grown by the Korea Research Institute of Chemical Technology.<sup>13</sup> The iron and aluminum impurities in this cultured quartz crystal were not purposely doped in, but are present because the Korean silica feedstock used contains mass ratio 68.2 ppm Fe to Si of  $\text{Fe}_2\text{O}_3$ ; some  $\text{Al}_2\text{O}_3$  was added when growing the crystal. Two cylindrical EPR samples were cut out of the original synthetic quartz crystal. The respective cylinder axes are approximately parallel to the threefold screw (optical) axis  $\hat{c}$  and one ( $\equiv \hat{a}_1$ ) of the twofold axes in the  $\alpha$ -quartz crystal. The samples have diameters of about 5.7 and 6.6 mm, respectively, and each has a length of about 15 mm. A fraction only of each crystal

was irradiated with x rays (tungsten target, 50 kV, 45 mA) for 20 min at room temperature to generate the well-characterized center  $[\text{AlO}_4]^{0,14}$  used for crystal alignment by EPR (x rays destroy the  $[\text{FeO}_4/\text{Li}]^0$  centers).

The Korean crystal was used for our measurements since centers  $\alpha'$  and  $\alpha''$  occurred with reasonably high concentrations, in some regions excised from it. These same centers were also seen in the yellow-brown iron-doped quartz<sup>4</sup> produced by Sawyer Research Products Inc. (Eastlake OH, USA), as were traces of still another center probably of the same type.

A right-hand orthogonal reference axis system  $XYZ$  was used, with  $\hat{X} \parallel \hat{a}_1$ ,  $\hat{Y} \parallel \hat{c} \otimes \hat{a}_1$ , and  $\hat{Z} \parallel \hat{c}$ , respectively, to describe the EPR spectral parameters. The orientation of the external magnetic field vector  $\hat{B} = \mathbf{B}/B$  is specified using polar angle  $\theta = \angle(\hat{Z}, \hat{B})$  and azimuthal angle  $\phi = \angle(\hat{X}, \text{the projection of } \hat{B} \text{ onto the } XY \text{ plane})$ . The two samples were mounted in the cylindrical EPR cavity such that  $\hat{c}$  and  $\hat{a}_1$ , respectively, were parallel to  $\hat{B}_1$  (microwave magnetic field) and perpendicular to  $\hat{B}_1$ . The alignment of the crystal was accurately adjusted ( $\pm 1$  min of arc), using the  $[\text{AlO}_4]^0$  spectra, for all orientations of  $\hat{B}$  in the horizontal plane.

EPR line-position data sets were collected at around 35 K using a previously described low-temperature EPR cavity system<sup>15</sup> and a Varian V4502 spectrometer operated at a frequency of around 9.90 GHz. Our frequency values and line-position field data have estimated uncertainties of  $1 \times 10^{-6}$  GHz and  $1 \times 10^{-3}$  mT, respectively. The magnetic field was measured using a proton NMR gaussmeter and was calibrated using the line positions of the  $[\text{AlO}_4]^0$  spectra at around 350 mT. A small linear correction was applied to all measured magnetic fields to take into account the difference in position between the NMR probe and the quartz sample.

The EPR spectra of the three centers  $\alpha$ ,  $\alpha'$  and  $\alpha''$  were reported to be visible in the temperature range 90–300 K and not to vary appreciably.<sup>12</sup> We now find no major change (and no symmetry breaking) down to 35 K.

Rotation data for the centers  $[\text{FeO}_4/\text{Li}]_{\alpha'}$  and  $[\text{FeO}_4/\text{Li}]_{\alpha''}$  (as well as for  $[\text{FeO}_4/\text{Li}]_{\alpha}$ ), were collected basically in  $10^\circ$  steps for all observable fine-structure lines, over a  $180^\circ$  range in the two crystallographic planes,  $XY$  (Fig. 1) and  $YZ$  (Fig. 2). Around the extrema and turning points of the fine-structure line positions, data points were collected at  $1^\circ$  intervals. Rotation patterns for  $\alpha'$  and  $\alpha''$  are represented by solid and dashed curves, respectively, in Figs. 1 and 2. These angular dependences are very similar to those of the  $[\text{FeO}_4/\text{Li}]_{\alpha}$  center (Figs. 1 and 2 in Ref. 3). However, center  $\alpha$  occurs in all symmetry-related sites 1, 2, and 3 (Ref. 16) corresponding to the centers located on the three equivalent twofold axes  $\hat{a}_1$ ,  $\hat{a}_2$ , and  $\hat{a}_3$ , respectively, whereas  $\alpha'$  and  $\alpha''$  exist in site 1 only in the EPR spectra observed in the Korean crystal. Here we have labeled as  $\hat{a}_1$  the electrical axis perpendicular to the largest surface in the traditional shape of a synthetic quartz crystal, grown from a seed plate with long dimension along  $\hat{Y}$ , and  $\hat{Z}$  perpendicular to the largest-area plane. Theoretically the three sites have equal probability of bearing  $\text{Fe}^{3+}$  centers, but in the

actual crystal, region-dependent site preferences were found. For instance, the spectral intensities of the  $\alpha$  center, for the three sites 1, 2, and 3, respectively, were found to have relative ratios of 10:1.2:0.8 in a sample of Brazilian natural amethyst<sup>9</sup> and 3.5:1.0:1.1 in our Korean synthetic quartz.<sup>11</sup> The two centers  $\alpha'$  and  $\alpha''$  have small abundances, approximately 13% and 16%, respectively, relative to that of  $\alpha$  (site 1), in a plate excised from the central section (with broad face perpendicular to  $\hat{Y}$ ) of the as-grown crystal.<sup>11</sup> In the Sawyer iron-doped cultured quartz,<sup>4</sup> they occur with one to two orders of magnitude less than the above percentages, but with approximately equal concentrations for all the symmetry-related sites.

The signal intensities of the three centers show a strong dependence on the location of the sample excised from the quartz crystal as grown. For example, when a sample, cut particularly such that the EPR signals of the two centers  $\alpha'$  and  $\alpha''$  showed large intensities, was mounted reversely with respect to its cylinder axis in the EPR cavity so that the opposite end of the sample was protruding into the cavity, the intensities of the two centers were strikingly reduced while that of  $\alpha$  was considerably increased. A separate publication describing distribution studies for these centers is being prepared.<sup>17</sup>

After taking the spin-Hamiltonian data, the sample was annealed for 20 h at a temperature of around 500 °C,

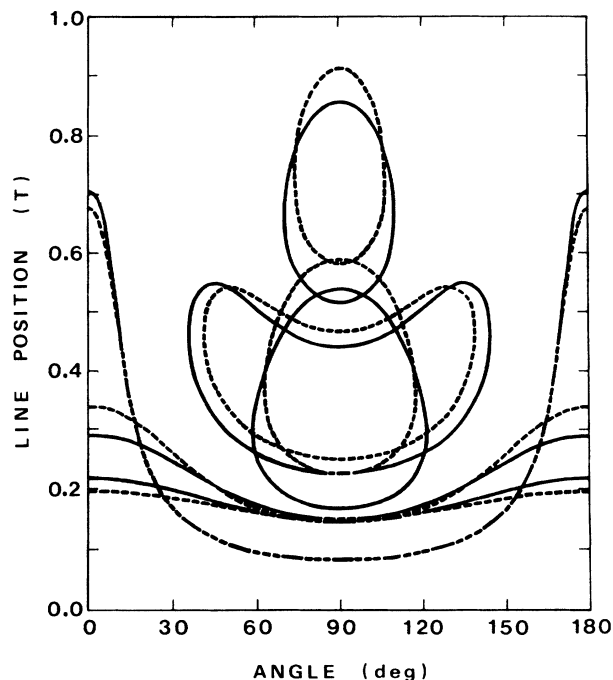


FIG. 1. Angular dependence of EPR line positions as a function of crystal rotation about threefold screw axis  $\hat{c}$ , at 9900 MHz and  $T \approx 35$  K, where the solid line represents  $[\text{FeO}_4/\text{Li}]_{\alpha'}$  and the dashed line  $[\text{FeO}_4/\text{Li}]_{\alpha''}$ . Here the centers are located on axis  $\hat{a}_1$ . At the field scale used, the  $^7\text{Li}$  hyperfine structure is not discernible and the long-short dashed line represents an overlap of the EPR line positions for the two centers. Angle  $0^\circ$  is at  $\hat{B} \parallel \hat{a}_1$ , and  $90^\circ$  is at  $\hat{B} \parallel \hat{Y}$  ( $\perp \hat{a}_1$  and  $\hat{c}$ ).

with the result that centers  $\alpha'$  and  $\alpha''$  were significantly reduced in signal intensity while the site-1  $\alpha$  concentration increased. This suggests that  $\alpha'$  and  $\alpha''$  were partly converted into  $\alpha$ . After a sample was electrodiffused with lithium ions for 8 h at around 400°C, with an applied electric field of around 50 V/cm along the axis  $\hat{c}$ , the intensities of all the three centers increased. The sample was then electrodiffused with sodium ions for 10 h at around 400°C, with an applied electric field of around 200 V/cm along the  $\hat{c}$ . This treatment resulted in a considerable decrease in the signal intensity of all three lithium centers, but caused a strong signal from the center  $[\text{FeO}_4/\text{Na}]^0$ ,<sup>7</sup> plus weak as yet uncharacterized signals. This experiment confirms that the three centers  $\alpha$ ,  $\alpha'$ , and  $\alpha''$  are compensated by the lithium  $1+$  ion.

The EPR linewidths depend somewhat on orientation, transition, and resonance field. The lines tend to be broadest at orientations where the slope of the line position versus angle (for rotation about  $\hat{c}$  and  $\hat{a}_1$ ) is steepest. The full linewidths between extrema of the first derivative for the three centers  $\alpha$ ,  $\alpha'$ , and  $\alpha''$ , respectively, vary from around 0.09, 0.11, and 0.11 mT for a fine-structure line in the lowest-field region to 0.60, 0.68, and 0.69 mT for the lines in the 1-T region.

At some orientations, hyperfine splittings from the  $^7\text{Li}$  nucleus ( $I = \frac{3}{2}$ , 92.5% abundance) for all the three centers were visible and measurable, using the data collection

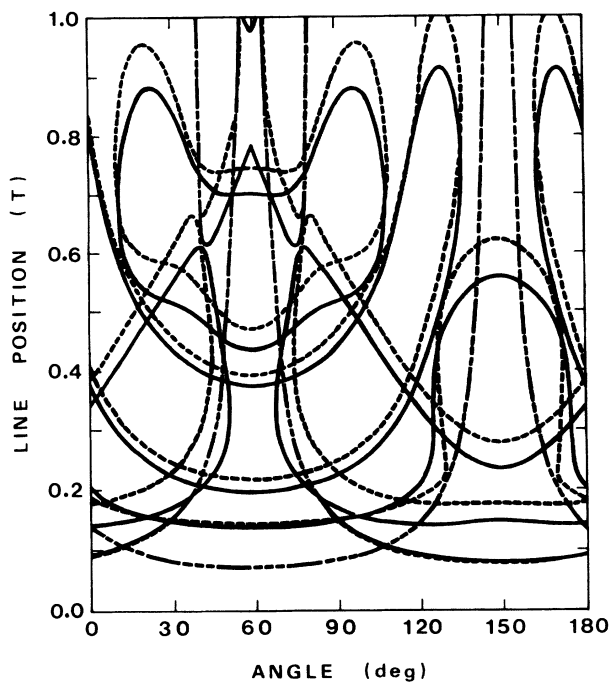


FIG. 2. Angular dependence of EPR line positions as a function of crystal rotation about twofold axis  $\hat{a}_1$ , at 9900 MHz and  $T$  = around 35 K, where the solid line represents  $[\text{FeO}_4/\text{Li}]_{\alpha}^0$  and the dashed line  $[\text{FeO}_4/\text{Li}]_{\alpha''}^0$ . Here the centers are located on axis  $\hat{a}_1$ . At the field scale used, the  $^7\text{Li}$  hyperfine structure is not discernible and the long-short dashed line represents an overlap of the EPR line positions for the two centers. Angle 0° is at  $\hat{B} \parallel \hat{c}$ , and 90° is at  $\hat{B} \parallel \hat{Y}$ .

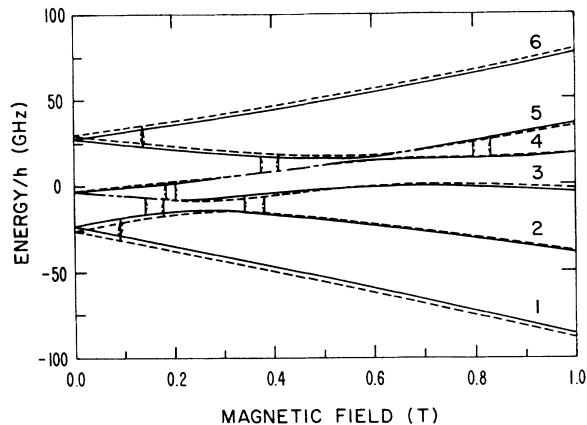


FIG. 3. The energy levels for the two centers  $[\text{FeO}_4/\text{Li}]_{\alpha}^0$  (solid line) and  $[\text{FeO}_4/\text{Li}]_{\alpha''}^0$  (dashed line) in site 1, as a function of external magnetic field  $B$  ( $\hat{B} \parallel \hat{c}$ ). The long-short dashed line represents an overlap of energy levels for the two centers at the energy scale used. The levels corresponding to the high-field  $m_s$  quantum numbers  $-\frac{5}{2}$ ,  $-\frac{3}{2}$ ,  $-\frac{1}{2}$ ,  $\frac{1}{2}$ ,  $\frac{3}{2}$ , and  $\frac{5}{2}$  are numbered in order (increasing energy) from 1 to 6. No hyperfine splittings are included. Transitions at 9900 MHz are indicated, and occur at (calculated) fields 92.95, 139.53, 142.13, 202.63, 341.56, 375.78, and 798.57 mT for  $[\text{FeO}_4/\text{Li}]_{\alpha}^0$ , and 90.03, 138.35, 178.94, 184.10, 383.07, 409.81, and 833.94 mT for  $[\text{FeO}_4/\text{Li}]_{\alpha''}^0$ .

method of multiple-scan storage. The  $^7\text{Li}$  hyperfine structure was most clearly seen on low-field EPR lines 3–4 (the transitions between states labeled with  $m_s = -\frac{1}{2}$  and  $\frac{1}{2}$  in the high-field-limit scheme; see Fig. 3). Hyperfine spectra for the three centers were collected from the 3–4 transitions at some angles in the  $XY$  plane near the  $\hat{a}_1$  axis (see Fig. 1) and in the  $YZ$  plane from  $\theta = 10^\circ$  to  $110^\circ$  (see Fig. 2).

### III. RESULTS AND DISCUSSION

The same spin-Hamiltonian form as used for  $[\text{FeO}_4/\text{Li}]_{\alpha}^0$  (Ref. 3) was utilized here, since all the three centers have the same  $C_2$  local symmetry. We have accurately determined the spin-Hamiltonian parameters including matrices  $\mathbf{g}$ ,  $\mathbf{D}$ ,  $\mathbf{A}(^7\text{Li})$ , and  $\mathbf{P}(^7\text{Li})$  as well as the conventional Stevens parameters  $B_4^n$  for  $S^4$  terms (Tables I and II). The matrices  $\mathbf{g}$ ,  $\mathbf{D}$  and the  $S^4$  parameters were obtained using 138 and 128 fine-structure line positions for the two centers  $[\text{FeO}_4/\text{Li}]_{\alpha}^0$  and  $[\text{FeO}_4/\text{Li}]_{\alpha''}^0$ , respectively. The final rms deviations between the observed and calculated EPR line positions were 0.062 mT and 0.064 mT, respectively. The hyperfine matrices  $\mathbf{A}(^7\text{Li})$  and the nuclear quadrupole matrices  $\mathbf{P}(^7\text{Li})$  for the three centers  $\alpha'$ ,  $\alpha''$ , and  $\alpha$  (Tables I, II, and III, respectively) were determined using 88, 116, and 130 individual line positions, respectively, taken from the low-field 3–4 transitions. In the subsequent fitting procedure, the lithium nuclear Zeeman matrix  $\mathbf{g}_n(^7\text{Li})$  was kept isotropic with  $g_n = 2.170961$ , and only the matrix elements of  $\mathbf{A}$  and  $\mathbf{P}$  were varied. In the case of the  $[\text{FeO}_4/\text{Li}]_{\alpha}^0$  center, the 20-K matrices  $\mathbf{g}$  and  $\mathbf{D}$  and the  $S^4$  parameters<sup>3</sup> were used. The final rms deviations for the three centers  $\alpha'$ ,

TABLE I. Center  $[\text{FeO}_4/\text{Li}]_a^0$  principal values and directions of matrices  $\mathbf{Y}=\mathbf{g}, \mathbf{D}, \mathbf{A}({}^7\text{Li})$ , and  $\mathbf{P}({}^7\text{Li})$  in the crystal Cartesian coordinate system<sup>a</sup> at around 35 K, derived from the EPR data. The  $S^4$  parameters  $B_4^m$  are included. The estimated statistical uncertainties in the last significant figures are appended, in parentheses.

Y		k		$Y_k$	$\theta_k$ (deg)	$\phi_k$ (deg)	
<b>g</b>							
2.004 24(14)	0	0	1	2.004 80(13)	39.8(3.9)	270	
	2.004 10(12)	-0.000 58(9)	2	2.004 24(14)	90	0	
		2.004 32(13)	3	2.003 62(12)	129.8(3.9)	270	
<b>D/h (MHz)</b>							
-1350.48(54)	0	0	1	5425.40(32)	120.716(3)	270	
	2946.72(59)	4171.85(41)	2	-1350.48(54)	90	0	
		-1596.24(48)	3	-4074.92(49)	30.716(3)	270	
<b>A(<sup>7</sup>Li)/h (MHz)</b>							
3.396(16)	0	0	1	3.396(16)	90	0	
	-1.032(12)	-0.152(26)	2	-0.724(37)	26.3(1.3)	270	
		-0.799(39)	3	-1.107(24)	116.3(1.3)	270	
<b>P(<sup>7</sup>Li)/h (MHz)</b>							
-0.037(23)	0	0	1	0.126(18)	104(5)	270	
	0.114(21)	0.050(15)	2	-0.037(23)	90	0	
		-0.077(24)	3	-0.089(21)	14(5)	270	
<b><math>B_4^m/h</math> (MHz)</b>							
$B_4^0/h$	0.57(1)						
$B_4^1/h$	0	$B_4^2/h$	-1.12(3)	$B_4^3/h$	0	$B_4^4/h$	4.60(11)
$B_4^{-1}/h$	4.40(9)	$B_4^{-2}/h$	0	$B_4^{-3}/h$	1.23(15)	$B_4^{-4}/h$	0

<sup>a</sup>Ref. 1, Table II, coordinate system (1); note that any principal direction defined by angles  $\theta_k$  and  $\phi_k$  equivalently can be described by angles  $180^\circ - \theta_k$  and  $180^\circ + \phi_k$ .

TABLE II. Center  $[\text{FeO}_4/\text{Li}]_a^0$  principal values and directions of matrices  $\mathbf{Y}=\mathbf{g}, \mathbf{D}, \mathbf{A}({}^7\text{Li})$  and  $\mathbf{P}({}^7\text{Li})$  in the crystal Cartesian coordinate system (see footnote, Table I) at around 35 K, derived from the EPR data. The  $S^4$  parameters  $B_4^m$  are included. The estimated statistical uncertainties are appended, in parentheses.

Y		k		$Y_k$	$\theta_k$ (deg)	$\phi_k$ (deg)	
<b>g</b>							
2.004 35(13)	0	0	1	2.004 88(14)	31.4(3.5)	270	
	2.003 85(12)	-0.000 63(11)	2	2.004 35(13)	90	0	
		2.004 50(12)	3	2.003 47(13)	121.4(3.5)	270	
<b>D/h (MHz)</b>							
-1123.24(53)	0	0	1	5847.65(39)	121.090(3)	270	
	3028.60(72)	4675.05(46)	2	-1123.24(53)	90	0	
		-1905.36(50)	3	-4724.41(47)	31.090(3)	270	
<b>A(<sup>7</sup>Li)/h (MHz)</b>							
3.497(8)	0	0	1	3.497(8)	90	0	
	-1.084(6)	-0.143(12)	2	-0.829(17)	29.3(9)	270	
		-0.910(18)	3	-1.165(12)	119.3(9)	270	
<b>P(<sup>7</sup>Li)/h (MHz)</b>							
0.089(12)	0	0	1	0.089(12)	90	0	
	-0.055(17)	-0.011(13)	2	-0.029(12)	23(29)	270	
		-0.034(17)	3	-0.060(11)	113(29)	270	
<b><math>B_4^m/h</math> (MHz)</b>							
$B_4^0/h$	0.57(1)						
$B_4^1/h$	0	$B_4^2/h$	-1.17(4)	$B_4^3/h$	0	$B_4^4/h$	4.93(12)
$B_4^{-1}/h$	4.08(8)	$B_4^{-2}/h$	0	$B_4^{-3}/h$	1.04(17)	$B_4^{-4}/h$	0

$\alpha''$ , and  $\alpha$  were 0.0020, 0.0015, and 0.0012 mT, respectively. The sets of spin-Hamiltonian parameters were chosen with signs such that the matrices  $\mathbf{D}$  match the one reported for  $[\text{FeO}_4/\text{Li}]_{\alpha}^0$  (Ref. 3). The signs of matrices  $\mathbf{A}({}^7\text{Li})$  and  $\mathbf{P}({}^7\text{Li})$  are thereby fixed, and are determined by the fitting procedure.

The sets of all possible site-1 EPR line positions for the two centers  $[\text{FeO}_4/\text{Li}]_{\alpha'}^0$  and  $[\text{FeO}_4/\text{Li}]_{\alpha''}^0$  within the magnetic-field range 0–1 T, for fixed microwave frequency 9900 MHz, are shown in Figs. 1 and 2 for rotation planes  $XY$  and  $YZ$ , respectively. The experimental data points do not deviate visibly from the calculated curves shown, on the field scale used. Energy-level diagrams are given in Fig. 3 as a function of magnetic field  $B$ , for  $\hat{\mathbf{B}}\|\hat{\mathbf{c}}$ , indicating EPR transitions occurring at 9900 MHz. Corresponding simulated  $c$ -axis spectra for the two centers (using the spin-Hamiltonian parameters in Tables I and II, respectively) are presented in Fig. 4.

To compare hyperfine spectra for the three centers, observed and calculated EPR spectra showing the best-resolved  ${}^7\text{Li}$  hyperfine structure observable in the  $YZ$  plane are given in Fig. 5. The simulation was done at experimental frequency 9898.67 MHz, assuming that all EPR lines in each center had the same linewidth ( $\Delta B_{p-p} = 0.014, 0.032, \text{ and } 0.032$  mT for  $\alpha, \alpha', \text{ and } \alpha''$ , respectively) and that the line shapes are Lorentzian first

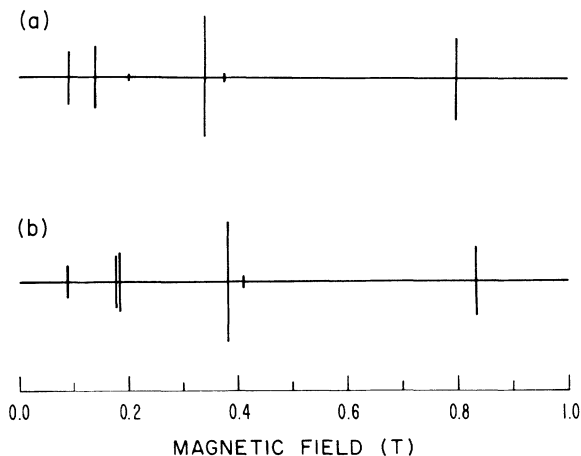


FIG. 4. EPR fine-structure spectra for  $[\text{FeO}_4/\text{Li}]_{\alpha}^0$  (a) and  $[\text{FeO}_4/\text{Li}]_{\alpha''}^0$  (b) at 9900 MHz simulated from the best-fit 35-K spin-Hamiltonian parameters in Tables I and II, respectively, for  $\hat{\mathbf{B}}\|\hat{\mathbf{c}}$  and excitation field  $\hat{\mathbf{B}}_1\|\hat{\mathbf{a}}_1$ . The transitions are also shown in Fig. 3. The  ${}^7\text{Li}$  hyperfine splitting is not visible at the field scale used. The spectrum agrees well with the observed one: The lines at 139.53 mT for  $[\text{FeO}_4/\text{Li}]_{\alpha}^0$  and at 138.35 mT for  $[\text{FeO}_4/\text{Li}]_{\alpha''}^0$  are not visible here due to their very small intensities.

TABLE III. Center  $[\text{FeO}_4/\text{Li}]_{\alpha}^0$  principal values and directions of matrices  $\mathbf{Y} = \mathbf{A}({}^7\text{Li})$  and  $\mathbf{P}({}^7\text{Li})$  in the crystal Cartesian coordinate system [Ref. 1, Table II, coordinate system (1)] for site 1 at around 35 K, derived from the EPR data. The estimated statistical uncertainties are included, in parentheses. The 20-K matrices  $\mathbf{g}$  and  $\mathbf{D}$  and parameters  $B_4^m$  from Ref. 3 are also tabulated.

	$\mathbf{Y}$		$k$	$Y_k$	$\theta_k$ (deg)	$\phi_k$ (deg)	
$\mathbf{g}$							
2.00426(49)	0	0	1	2.00426(49)	90	0	
	2.00370(21)	0.00022(11)	2	2.00418(17)	25.0(12.0)	90	
		2.00408(19)	3	2.00360(19)	115.0(12.0)	90	
$\mathbf{D}/h$ (MHz)							
-1399.79(51)	0	0	1	6348.35(68)	119.699(3)	270	
	3575.44(75)	4861.72(54)	2	-1399.79(51)	90	0	
		-2175.65(72) <sup>a</sup>	3	-4948.56(68)	29.699(3)	270	
$\mathbf{A}({}^7\text{Li})/h$ (MHz)							
3.643(6)	0	0	1	3.643(6)	90	0	
	-0.870(5)	-0.134(10)	2	-0.630(15)	29.2(7)	270	
		-0.705(15)	3	-0.945(10)	119.2(7)	270	
$\mathbf{P}({}^7\text{Li})/h$ (MHz) <sup>b</sup>							
0.005(6)	0	0	1	0.011(7)	15(18)	270	
	-0.014(8)	-0.007(8)	2	0.005(6)	90	0	
		0.009(7)	3	-0.015(8)	105(18)	270	
$B_4^m/h$ (MHz)							
$B_4^0/h$	0.513(15)						
$B_4^1/h$	0	$B_4^2/h$	-1.238(55)	$B_4^3/h$	0	$B_4^4/h$	3.812(85)
$B_4^{-1}/h$	3.800(80)	$B_4^{-2}/h$	0	$B_4^{-3}/h$	0.400(24)	$B_4^{-4}/h$	0

<sup>a</sup>The value given for this element in Ref. 3 is in error.

<sup>b</sup>The sign of this matrix is opposite to the one listed in Ref. 3. The present fitting yields the sign as given above (with a slightly lower root-mean-square deviation than is obtained with the old opposite choice).

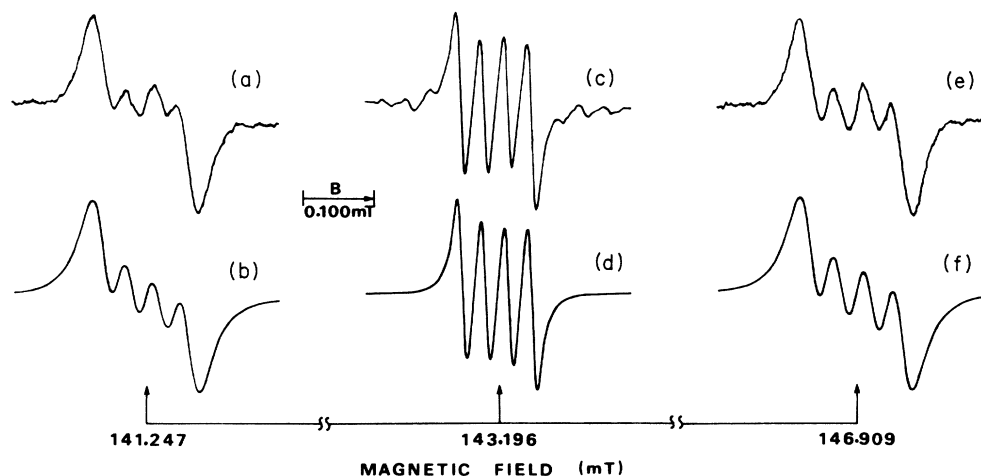


FIG. 5. First-derivative 35-K EPR spectra at 9898.67 MHz, showing the  ${}^7\text{Li}$  hyperfine lines of the low-field 3–4 ( $m_s: -\frac{1}{2}$  to  $\frac{1}{2}$ ) transition at crystal orientation  $\theta=80^\circ$ ,  $\phi=90^\circ$ . Parts (a), (c), and (e) represent experimental (site 1) spectra for  $[\text{FeO}_4/\text{Li}]_{\alpha}^0$ ,  $[\text{FeO}_4/\text{Li}]_{\alpha'}^0$ , and  $[\text{FeO}_4/\text{Li}]_{\alpha''}^0$ , respectively. Parts (b), (d), and (f) show spectra simulated from the spin-Hamiltonian parameters of Table I, Table III, and Table II, for the above three centers, respectively.

derivatives. The outer weak signals on each side of the primary spectrum in Fig. 5(c) are thought to originate from  ${}^{29}\text{Si}$  ( $I=\frac{1}{2}$ , 4.67% abundance) plus  ${}^7\text{Li}$ . The spacing of around 0.21 mT of this pair of quartets is the same as that (around 0.22 mT) of the  ${}^{29}\text{Si}$  doublet previously seen<sup>3</sup> in  $[\text{FeO}_4/\text{Li}]_{\alpha}^0$ , and the splitting of around 0.03 mT between individual signals is that of the  ${}^7\text{Li}$  quartet. The intensity of each weak quartet is about 4.8% relative to that of main quartet. This value is reasonable, considering the natural abundance of  ${}^{29}\text{Si}$  and the twofold symmetry of the Si site in the crystal. The observed slight asymmetry within each quartet in the experimental spectra may arise from the  ${}^6\text{Li}$  hyperfine spectrum.<sup>3</sup> Similar splittings were poorly resolved for the other two centers because of the low signal intensities.

The principal  $g$  values for  $[\text{FeO}_4/\text{Li}]_{\alpha'}^0$  and  $[\text{FeO}_4/\text{Li}]_{\alpha''}^0$  (Tables I and II, respectively) do not differ much from those of  $[\text{FeO}_4/\text{Li}]_{\alpha}^0$ .<sup>3</sup> They are almost isotropic and the principal values all are close to (and are slightly greater than) the free-electron value  $g_e$ , as is reasonable for a covalently bonded  $S$ -state ion.<sup>18</sup> Their two principal axis directions perpendicular to the  $\hat{a}_1$  axis are different from those of the  $[\text{FeO}_4/\text{Li}]_{\alpha}^0$  center (but may be related to them by a mirror reflection in the  $XZ$  plane). The principal directions of matrices  $\mathbf{g}$  for the two centers are almost coincident with those of the matrices  $\mathbf{D}$  and also are close to those of the “symmetrized” matrices  $\mathbf{D}_{\text{sym}}$  [i.e., matrices averaged over the two (twofold) symmetry-related sites (configurations) 1 and 1'] of the centers  $[\text{FeO}_4/\text{Li}]_{\beta}^0$  (see Ref. 4, Table II) and  $[\text{FeO}_4/\text{Na}]^0$  (see Ref. 7, Table II).

We note that there is almost perfect coincidence in the principal directions of the electronic quadrupole matrices  $\mathbf{D}$  for the two centers  $[\text{FeO}_4/\text{Li}]_{\alpha'}^0$  and  $[\text{FeO}_4/\text{Li}]_{\alpha''}^0$  with those of  $[\text{FeO}_4/\text{Li}]_{\alpha}^0$ , but not with those<sup>4</sup> of  $[\text{FeO}_4/\text{Li}]_{\beta}^0$ . Thus we identify the two centers  $\alpha'$  and  $\alpha''$  as being of type  $\alpha$ , and conclude that the two centers have a closely similar local configuration to that of  $[\text{FeO}_4/\text{Li}]_{\alpha}^0$ . For the

three centers, it is of interest to compare the uniaxiality ( $D$ ) and the rhombicity ( $E$ ) parameters [defined, respectively, as  $D=3D_1/(2h)$ ,  $E=(D_2-D_3)/(2h)$ , where  $D_k$  ( $k=1,2,3$ ; see Tables I–III) are the principal values of matrix  $\mathbf{D}$  obeying the condition  $|D_1| \geq |D_2| \geq |D_3|$ ] and the ratio  $|E/D|$  (ranging from 0 to  $\frac{1}{3}$ , for ideally uniaxial and rhombic matrices  $\mathbf{D}$ , respectively). They are as follows:  $D/h=9522.5(10)$ , 8138.1(5), and 8771.5(6) MHz;  $|E/h|=1774.4(6)$ , 1362.2(5), and 1800.6(5) MHz; and  $|E/D|=0.1863(1)$ , 0.1674(1), and 0.2053(1), for  $[\text{FeO}_4/\text{Li}]_{\alpha}^0$  (at 20 K),  $[\text{FeO}_4/\text{Li}]_{\alpha'}^0$  (at 35 K), and  $[\text{FeO}_4/\text{Li}]_{\alpha''}^0$  (at 35 K), respectively. The  $D$  values are in descending order for  $\alpha$ ,  $\alpha'$ , and  $\alpha''$ , whereas the  $|E/D|$  ratios are in ascending order for  $\alpha'$ ,  $\alpha$ , and  $\alpha''$ .

In the temperature range 90–300 K, the parameters  $D$  and  $E$  decrease linearly with increasing temperature, at small rates.<sup>12</sup> Extrapolation of the parameters to 35 K yields the following:  $D/h=9538$ , 8145, and 8825 MHz, and  $|E/h|=1815$ , 1401, and 1857 MHz, respectively, for  $\alpha$ ,  $\alpha'$ , and  $\alpha''$ . These agree reasonably well with our present experimental values, showing that no major thermal effects (such as are found<sup>4,5</sup> in  $[\text{FeO}_4/\text{Li}]_{\beta}^0$  and  $[\text{FeO}_4/\text{Na}]^0$ ) occur between 35 and 300 K.

Comparison of the sets of electronic hexadecapole parameters  $B_4^m$  in Tables I–III reveals that these are close to being the same for the three centers  $\alpha$ ,  $\alpha'$ , and  $\alpha''$ . These parameters are more sensitive to details of the iron ion's surroundings than are the quadrupole parameters  $D$  (or is matrix  $\mathbf{g}$ ), although they are not as accurately determined.

The matrices  $\mathbf{A}({}^7\text{Li})$  and  $\mathbf{P}({}^7\text{Li})$  of  $[\text{FeO}_4/\text{Li}]_{\alpha}^0$  (Table III) derived from the EPR data at 35 K agree well with those (Table II in Ref. 3) obtained from the ENDOR data at 4 K. The principal directions of matrices  $\mathbf{A}$  for the three centers  $\alpha$ ,  $\alpha'$ , and  $\alpha''$  (Tables III, I, and II, respectively) are close to coincident with the principal directions of  $\mathbf{D}$ , and are close also to those of  $\mathbf{P}$ . Note that the nuclear quadrupole effects are very small, near the limits

of our experimental accuracy. Matrices  $\mathbf{A}({}^7\text{Li})$  have isotropic parts [ $a_{\text{iso}} = \text{Tr } \mathbf{A}/(3h) = 0.689(10)$ ,  $0.522(26)$ , and  $0.501(12)$  MHz at around 35 K for  $\alpha$ ,  $\alpha'$ , and  $\alpha''$ , respectively] and are nearly uniaxial. Here we have chosen the sign of each matrix  $\mathbf{A}({}^7\text{Li})$  such that the uniaxiality parameter

$$b = [A_1 - (A_2 + A_3)/2]/(3h)$$

is positive, as expected for the magnetic dipole-dipole interaction.<sup>19</sup> These are 1.477(6), 1.437(16), and 1.498(8) MHz, for  $\alpha$ ,  $\alpha'$ , and  $\alpha''$ , respectively, whereas the asymmetry parameters  $c = (A_2 - A_3)/(2h)$  are only 0.158(13), 0.192(31), and 0.168(15) MHz, respectively. Here  $A_k$  ( $k = 1, 2, 3$ ) are the principal values of  $\mathbf{A}({}^7\text{Li})$  arranged in the order  $|A_1| \geq |A_3| \geq |A_2|$  (Tables I–III). The point-point dipolar model leads to iron-lithium distances of 2.75(1), 2.78(3), and 2.74(1) Å for  $\alpha$ ,  $\alpha'$ , and  $\alpha''$ , respectively. Use of this model seems reasonable here in view of the  $s$ -like electron distribution on both ions. The above distances agree well with the value of 2.61 Å (30–295 K) for the distance between atom Si(0) and the nearby interstitial  $a_{>}$  site in the pure  $\alpha$ -quartz structure.<sup>20</sup> The distance (2.30 Å) between Si(0) and the  $a_{<}$  site seems too small, as compared with the above calculated values. We note that the largest-magnitude principal values of matrices  $\mathbf{P}({}^7\text{Li})$  for the two centers  $\alpha'$  and  $\alpha''$  are 8 and 6 times, respectively, those for center  $\alpha$ . This suggests that the lithium 1+ ions in  $\alpha'$  and  $\alpha''$  are under the influence of larger electric-field gradients than in  $\alpha$ .

Herein we have presented accurate characterization of three very similar Fe<sup>3+</sup> centers, and have demonstrated that all three are Li<sup>+</sup>-compensated species. All three exhibit twofold symmetry about the crystal electric axis bearing the Fe<sup>3+</sup> and Li<sup>+</sup> (on the time average), over the broad temperature range 35–300 K. Judging from the

<sup>7</sup>Li parameter matrices, all three centers contain close-to-equal Fe-Li distances and directions.

The existence of the “additional” centers  $\alpha'$  and  $\alpha''$  of the type  $[\text{FeO}_4/\text{Li}]_{\alpha}^0$  is at this time difficult to rationalize. The sharpness of their EPR lines, the same as that of the  $\alpha$  center, indicates that the local surroundings are equally well defined and equivalent in all three centers. Certainly the EPR properties of the three are strikingly similar (Tables I–III). The tendency for distribution in separate regions of the crystal suggests that there may be differences generated at the time of crystal growth, which persist. The spectral occurrence for  $\alpha'$  and  $\alpha''$  of only some of the complete set of symmetry-related sites seems consistent with this, and indicates either lack of Fe<sup>3+</sup> population on some of the crystal twofold symmetry axes (electric axes  $\hat{a}_i$ , where  $i = 1, 2, 3$ ) or else broadening beyond observability of the EPR lines arising from the ferric ions residing on these axes. The explanation may involve the presence of appreciable and sharply defined internal electric fields along the twofold axes, differing for the three directions within the domains. Such fields could well cause the matrices  $\mathbf{D}$  to be substantially different,<sup>21</sup> as is observed for centers  $\alpha$ ,  $\alpha'$ , and  $\alpha''$ . Clearly, further experimentation is called for, and is under way.

#### ACKNOWLEDGMENTS

This work was supported in part by the Natural Sciences and Engineering Research Council of Canada, and by the Yonam Foundation of Korea. We are grateful to P. Bailey, G. Rogers, R. J. McEachern, M. J. Mombourquette, and J. A. S. Williams for the assistance they gave. We thank the Korea Institute of Chemical Technology, and Sawyer Research Products Inc., for making available iron-doped quartz crystals.

\* Author for correspondence.

<sup>1</sup>M. J. Mombourquette, W. C. Tennant, and J. A. Weil, *J. Chem. Phys.* **85**, 68 (1986).

<sup>2</sup>M. J. Mombourquette, J. Minge, M. R. Hantehzadeh, J. A. Weil, and L. E. Halliburton, *Phys. Rev. B* **39**, 4004 (1989).

<sup>3</sup>L. E. Halliburton, M. R. Hantehzadeh, J. Minge, M. J. Mombourquette, and J. A. Weil, *Phys. Rev. B* **40**, 2076 (1989).

<sup>4</sup>J. Minge, J. A. Weil, and D. G. McGavin, *Phys. Rev. B* **40**, 6490 (1989).

<sup>5</sup>J. Minge, M. J. Mombourquette, and J. A. Weil, *Phys. Rev. B* **40**, 6523 (1989).

<sup>6</sup>J. Minge and J. A. Weil, *J. Phys. Chem. Solids* **50**, 997 (1989).

<sup>7</sup>J. Minge, M. J. Mombourquette, and J. A. Weil, *Phys. Rev. B* **42**, 33 (1990).

<sup>8</sup>D. R. Hutton, *Phys. Lett.* **12**, 310 (1964).

<sup>9</sup>T. I. Barry, P. McNamara, and W. J. Moore, *J. Chem. Phys.* **42**, 2599 (1965).

<sup>10</sup>C. S. Han and S. H. Choh, *J. Korean Phys. Soc.* **22**, 241

(1989).

<sup>11</sup>D. Choi and S. H. Choh, *J. Korean Phys. Soc.* **21**, 107 (1988).

<sup>12</sup>D. Choi and S. H. Choh, *J. Phys. Condens. Matter* **1**, 7661 (1989).

<sup>13</sup>R. H. Park, *Korea Research Institute of Chemical Technology Newsletter* **2**, 10 (1980).

<sup>14</sup>R. H. D. Nuttall and J. A. Weil, *Can. J. Phys.* **59**, 1696 (1981).

<sup>15</sup>B. D. Perlson and J. A. Weil, *Rev. Sci. Instrum.* **46**, 874 (1975).

<sup>16</sup>J. A. Weil, T. Buch, and J. E. Clapp, *Adv. Magn. Reson.* **6**, 183 (1973).

<sup>17</sup>D. Choi, S. H. Choh, and R. H. Park (unpublished).

<sup>18</sup>M. Moreno, *Chem. Phys. Lett.* **76**, 597 (1980).

<sup>19</sup>M. J. Mombourquette and J. A. Weil, *J. Magn. Reson.* **66**, 105 (1986).

<sup>20</sup>J. A. Weil, *Phys. Chem. Miner.* **10**, 149 (1984).

<sup>21</sup>E. B. Royce and N. Bloembergen, *Phys. Rev.* **131**, 1912 (1963).